Surfaces and Interfaces 31 (2022) 102073

Contents lists available at ScienceDirect

Surfaces and Interfaces

journal homepage: www.sciencedirect.com/journal/surfaces-and-interfaces

Design rules for defect-free 3D perovskite-perovskite interfaces

Sundheep R, Ankit Jain *

Mechanical Engineering Department, Indian Institute of Technology, Bombay, India

ARTICLE INFO

Keywords:
Density functional theory
Perovskites
Interfacial defects

ABSTRACT

The understanding of defect dynamics at all 3D (bulk phase) hybrid organic-inorganic perovskite heterojunctions is necessary for improving the stability and performance of perovskite based devices. In this work, using density functional theory calculations, we study the effect of interfacial defects on the stability and electronic properties of a bromine based lead-tin perovskite heterojunction. We find that antisite defects are not stable at this interface and relax to form Pb/Sn interstitial and halide vacancy defects. Interstitial Pb/Sn defects result in the formation of dimer bonds along with associated mid bandgap states. The halide vacancy defects enhance the interaction between the neighboring B site cations at the interface and result in the formation of charge localizing mid bandgap states. Our results indicate that the bulk Pb-Sn perovskite heterojunction is vulnerable to the formation of charge localizing interfacial defects and adopting a Br rich synthesis condition is necessary to obtain a heterojunction with promising optoelectronic properties.

1. Introduction

With their superior optoelectronic properties and ease of fabrication at room temperature, organic-inorganic halide perovskite has been envisioned as an impending material for application in solar cells [1,2], light-emitting devices [3], lasers [4], detectors [5,6], and transistors [7]. These devices exhibit promising performance in various device architectures and employ heterojunctions between different materials. The imminent adaptation of these devices in commercial applications is currently hampered by their stability issues and lead (Pb) content associated toxicity. Perovskite composition and interface engineering are proposed as two effective strategies in this regard.

Initial studies suggested that mixed halide hybrid perovskites (ABX_3) where I^- at X position in methylammonium lead iodide ($MAPbI_3$) is substituted by Br^- or Cl^-can be employed to achieve high device performance along with improved stability under the ambient conditions [8]. Compared to $MAPbI_3$, $MAPbBr_3$ is environmentally more stable [9], results in higher open-circuit voltage [10], exhibits high absorption coefficients [11], and is optimal for application in tandem and triple-junction solar cells [12]. Further, tin based perovskites ($ASnX_3$) are proposed as an alternative to mitigate the Pb-toxicity in Pb-based perovskites. Notably, a piezoelectric generator with better ambient stability and mechanical durability is realized by employing $MASnBr_3$ in place of $MAPbI_3$, demonstrating the versatility of compositional engineering for device performance and stability enhancement [13]. The photo conversion efficiencies (PCE) so far achieved with pure Sn-based perovskite solar cells (PSCs), however, has been low due to the spontaneous oxidation of Sn^{2+} to Sn^{4+} at room temperature. The synergies of Pb- and Sn- based perovskites are utilized in mixed Pb-Sn perovskites where Br passivation reduces the lower dark current density and results in PCEs in excess of 19% [14].

The studies targeted towards device interface engineering focussed primarily on multi-dimensional perovskite (MDP) interfaces made up of a lower-dimensional perovskite (0D, 1D, or 2D) phase and 3D (bulk) phase. Pb-free PSCs demonstrating efficiencies in the range of 9% are achieved by carefully designing the 2D/3D interface [15,16]. The Br doping in the 2D perovskite capping layer part of the 2D/3D MDP interface resulted in an interfacial defect passivation with enhanced photoluminescence lifetimes and PCE of 20% [17]. A bilayer interdiffusion growth process for synthesis of Pb-Sn mixed perovskite when combined with a 1D pyrrolidinium perovskite based film passivation resulted in perovskite films with carrier lifetimes of 1.1 μs and PSCs of more than 20% PCE [18]. The extensive research studies on MDP interfaces have resulted in devices with enhanced stability and performance but similar studies are limited for all bulk phase perovskite heterojunctions [19].

All perovskite heterojunctions with the same phase (bulk 3D phase) on either side of the interface can be experimented to achieve the advantages of interface engineering and optimization of individual layer properties. The initial stagnation towards the development of all

* Corresponding author.
E-mail address: a_jain@iitb.ac.in (A. Jain).

https://doi.org/10.1016/j.surfin.2022.102073
Received 15 February 2022; Received in revised form 18 May 2022; Accepted 24 May 2022
Available online 27 May 2022

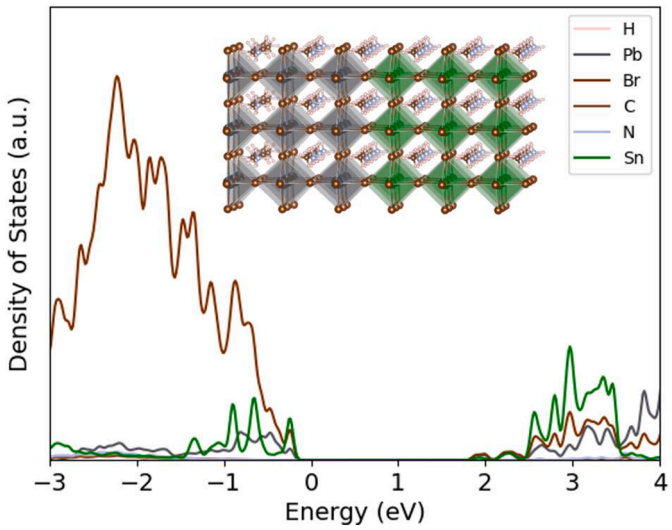

Fig. 1. The DOS of pristine $MAPbBr_3$-$MASnBr_3$ interface. The inset image shows $MAPbBr_3$-$MASnBr_3$ interface employed in this study. The interface is formed between 100 facets of cubic phases of $MAPbBr_3$ and $MASnBr_3$.

perovskite interface was associated with the difficulty in perovskite multilayer fabrication and facile ionic migration existing in these materials [20]. These initial challenges are now mastered and the recent forays to experimentally synthesise these heterojunctions have been highly encouraging [19]. In particular, a sequential solution and vapor processing method to create an all-bulk perovskite heterojunction is shown to create synergy between composition and grain size engineering and enabled the formulation of general design rules for fabricating perovskite-perovskite heterojunctions [19]. A solution-phase sequential growth approach enabled the fabrication of 2D perovskite based lateral heterostructures with an atomically sharp interface [21]. Replacing the charge transporting layers used in perovskite LEDs with $MAPbCl_3$ drives the conformal deposition of light-emitting $CsPbBr_3$ layers without increasing the driving voltage [22].

While mixed Pb-Sn perovskites have received considerable attention for their application in PSCs, bi-layer Pb-Sn perovskite interfaces have been rarely studied [23]. A recent experimental study reported that $MAPbBr_3$-$MASnBr_3$ interface exhibits ambient atmospheric stability of more than 1500 h demonstrating the sturdiness of the bi-layer interface [19]. DFT-based studies can be effectively utilized to obtain a mechanistic understanding of all perovskite heterojunctions aiding the experiments in robust heterojunction design with desired optoelectronic properties [24,25]. For $MAPbI_3$-$CsPbI_3$ superlattices, such DFT-based study suggested that vacancy defects have shallow transition states and the activation barrier for halide ion migration is high across the interface, indicating the beneficial impact of interface formation towards the stability enhancement of the PSC device which was later confirmed in experiments [26,27].

In this work, we employ DFT calculations to study the interface formation between Br-based lead- and lead-free perovskites, namely, $MAPbBr_3$ and $MASnBr_3$. The effect of interfacial defects on the stability and electronic properties of all perovskite heterojunction is examined by creating interfacial antisite, interstitial, and vacancy defects.

2. Computational details

The DFT calculations are performed using a Perdew Burkew Ernzerhof generalized gradient exchange correlation functional with plane-wave basis set and projected augmented wave pseudopotential as implemented in Vienna Ab Initio Simulation Package [28,29]. The plane-wave kinetic energy cut-off is fixed at 400 eV, and the Van der Waals interactions are modeled using the DFT-D3 method of Grimme [30]. The structure relaxation is carried out by sampling the electronic Brillouin zone corresponding to simulation supercell with a Gamma-only wavevector grid, and using an electronic convergence criterion of 10^{-5} eV per formula unit. All degrees of freedom including atomic positions, cell shape, and cell volume are allowed to change during the structure relaxation to minimize forces to less than 0.05 eV/Å. All geometry optimizations are performed without including the effect of spin-orbit coupling (SOC), while the SOC is taken into consideration during the density of states (DOS) calculation for pristine and defective interfaces. A minimum vacuum of 15 Å is ensured in the direction perpendicular to the interface in all calculations.

Previous studies have reported that at ambient pressure, $MASnBr_3$ exists in its cubic phase (pm3′m space group) and a stable heterojunction between $MAPbBr_3$ and $MASnBr_3$ in their pm3′ m cubic structure was experimentally realized [19,31]. Further, it was experimentally observed that $MASnBr_3$ perovskite films preferentially grow along (100) direction over indium tin oxide thin films [32]. Considering these facts, an all-perovskite interface is created by modeling a $3 \times 3 \times 3$ supercell of the (100) surface of $MAPbBr_3$ with a $3 \times 3 \times 3$ supercell of the (100) surface of $MASnBr_3$ consisting of a total of 648 atoms (Fig. 1).

The antisite defects (AD) are created at the interface by randomly exchanging the positions of interfacial Br atom with the Pb/Sn atom. Interstitial defects (ID) are generated by introducing an additional Br/Pb/Sn atom (charged ID) or by shifting the respective atoms from their original position to the interface (charge neutral ID). Vacancy defects (VD) are created by randomly removing the desired specie atom from the interface. Consequently, VD are charged defects, AD are charge-neutral defects and IDs have both charge neutral and charged compositions. For the AD and VD three random defect configurations are created for each defect, while four and six random defect configurations are generated for charged and uncharged ID, respectively.

The formation energies of the pristine interface is obtained as

$$E_{FE} = \frac{E_{Interface} - E_{surface1} - E_{surface2}}{S} \quad (1)$$

where $E_{FE}$is the formation energy of the pristine interface, $E_{Interface}$ is the relaxed energy of the interface, $E_{surface1}$and $E_{surface2}$ are the relaxed energy of the first and second molecular material surface which make up the interface, respectively, and S is the total surface area of the interface supercell. FE of defective interfaces are calculated by subtracting the relaxed energies of defective supercells from their pristine supercell counterparts. Out of the similar defect configurations, the defects having the lowest FE (most stable) values are used for analysis.

The density of states (DOS) is obtained by including the spin-orbit coupling to identify the defects with mid bandgap electronic states. Wavefunction visualization happening at the defect position is employed to understand the charge carrier localization at the defective interfaces. The inverse participation ratio (IPR) of the defective states is calculated to quantify the extent of wavefunction localization. The lower IPR value corresponds to a completely delocalized state while an increase in IPR value is indicative of the localization happening at the defective site [33,34].

3. Results and discussions

We begin our analysis by evaluating the formation energy of all-3D perovskite $MAPbBr_3$ –$MASnBr_3$ interface. It was previously reported in the literature that the preferential orientation for the case of $MAPbBr_3$ interface is MABr and as such the interface is created between $MAPbBr_3$ and $MASnBr_3$ with MABr and $SnBr_2$ termination, respectively [35,36]. The formation energy of the pristine interface as obtained from Eq. (1) is -2.11 eV/nm^2 which is comparable to that of a 2D/3D perovskite heterojunction (-3.06 eV/nm^2) [37] indicating that the interface is highly likely to form and is inherently stable.

The DOS of the pristine interface is shown in Fig. 1. The valence band

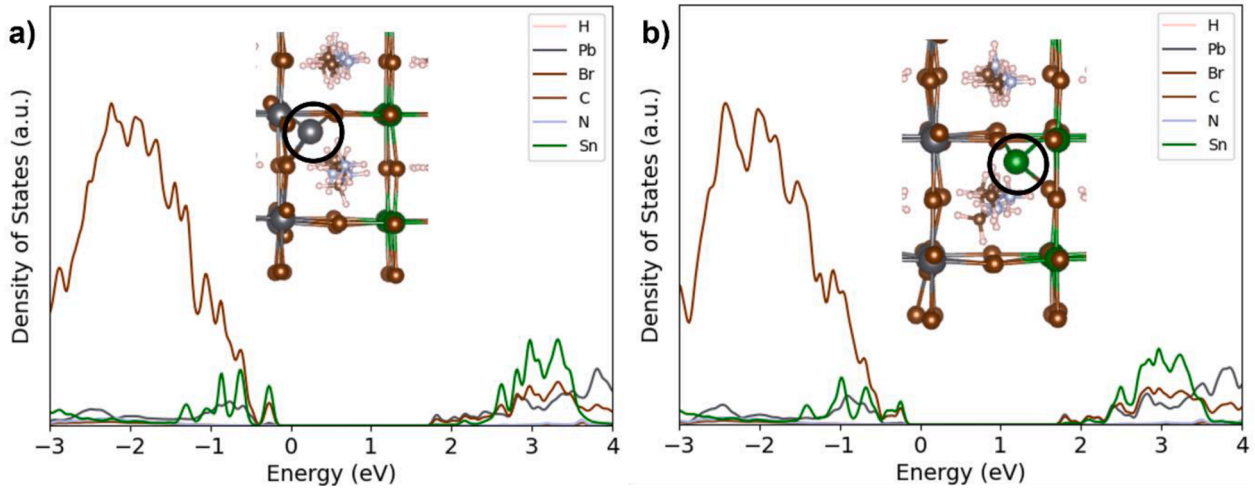

Fig. 2. The DOS of (a) Pb and (b) Sn AD at the $MAPbBr_3$-$MASnBr_3$ interface. The inset image shows the relaxed defect configurations of the corresponding interface where the black circle indicates an interstitial Pb/Sn atom. The interfacial AD relaxes into an Interstitial Pb/Sn and a halide vacancy defect configuration.

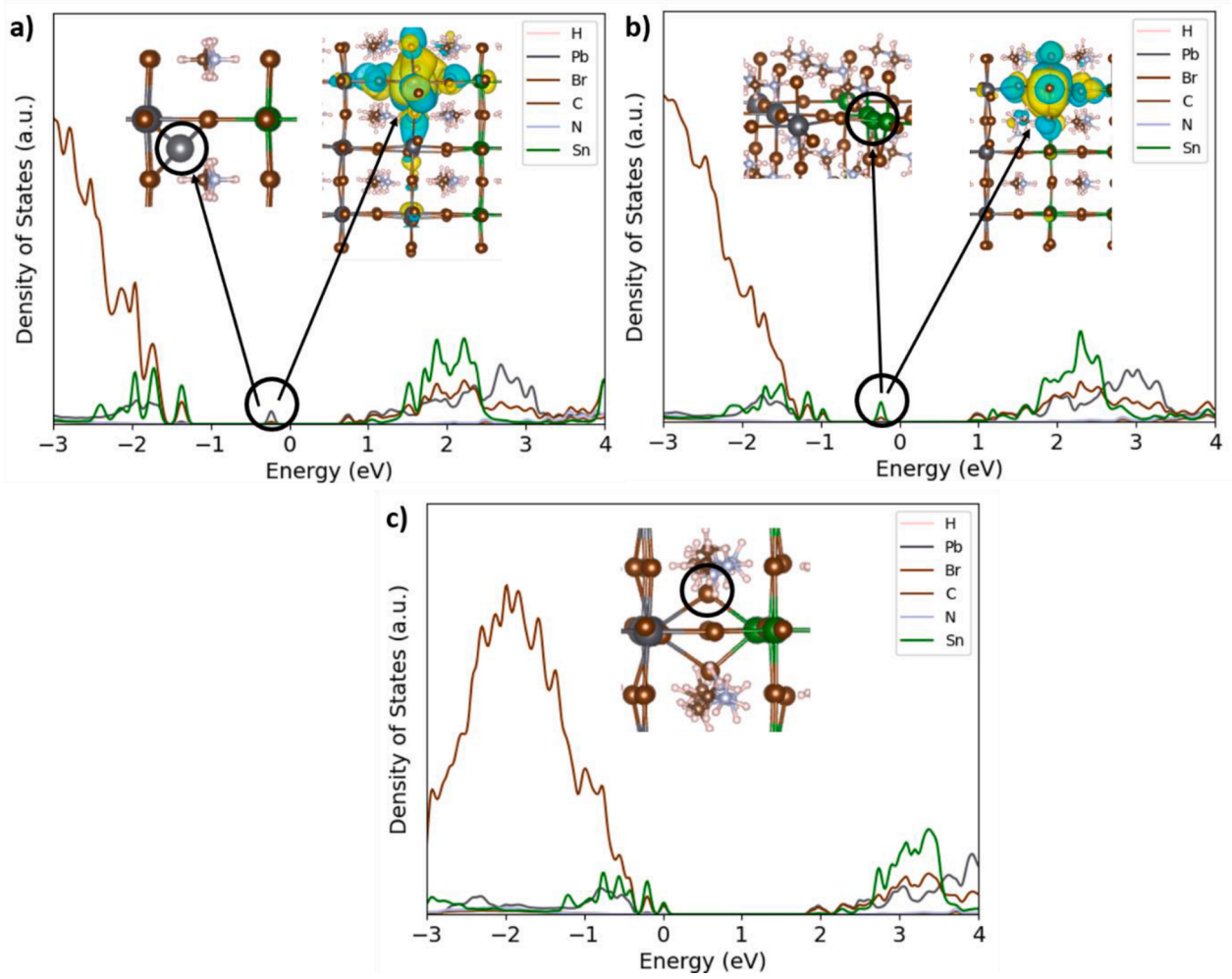

Fig. 3. The DOS of charged (a) Pb, (b) Sn and (c) Br ID at the $MAPbBr_3$-$MASnBr_3$ interface. The inset image shows the relaxed defect configurations at the interface where the black circle indicates an interstitial Pb/Sn/Br atom. Top right inset image in (a), (b) shows the wavefunction localization happening at the interfacial Pb, Sn ID site. Pb/Sn ID leads to the formation of mid bandgap states and charge localization while halide ID in (c) leads to the formation of a bridge atomic configuration without formation of mid bandgap states.

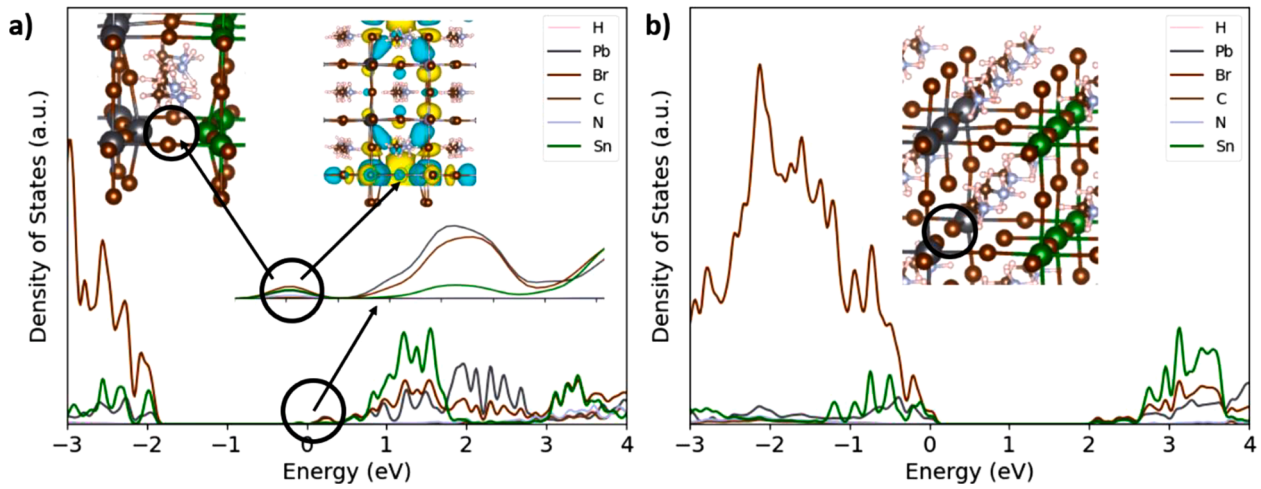

Fig. 4. The DOS of (a) Br and (b) Pb VD formed at the $MAPbBr_3$-$MASnBr_3$ interface. The top left inset image shows the relaxed defect configuration of VD where the black circle indicates the position of a Br/Pb vacancy. In figure (a) top middle inset image shows the wavefunction localization, and bottom right inset image shows the zoomed image of the mid bandgap state and the inset image in figure (b) shows the relaxed defect configuration of VD. Br VD at the interface lead to the formation of a midgap state resulting in significant charge carrier localization.

states are found to be dominated by the Sn orbitals with significant contribution from Br orbitals while conduction band states originate mainly from the Pb/Sn atoms. The inclusion of equal amounts of Sn to Pb-based perovskite introduces strongly hybridized Sn orbitals to the top of the valence band, which is clearly observable in Fig. 1. [38]

Moving forward, we next focus on charge-neutral AD. The negative FEs indicate that Pb (−1.23 eV) and Sn (−1.73 eV) AD are likely to form at the interface though, as can be seen from Fig. 2a and b, the formation of such defects does not result in any midgap states. The relaxed configuration of these defects show they are not stable and decompose into a combination of vacancy and interstitial defect as reported previously (Fig. 2a & b) [39]. The interstitial Pb/Sn atom forms bonds with the nearby Br atoms resulting in the formation of an interfacial $PbBr_3^-$ unit with reduced bond lengths (Fig. 2). The Pb-Br bond length for the pristine interface is 3.05 Å and it reduces to 2.81 Å for interface with AD defects. Similarly, in the case of Sn AD, the Sn-Br bond length reduces from 2.95 Å to 2.67 Å in defective configuration. The reduced Pb/Sn-Br bond lengths was associated with formation of deep level defects in the case of lead tri-halide perovskites which is not observed in Fig. 2. [40]. Similarly, bond length reduction with the formation of secondary tin phases MA_2SnI_6 and SnI_4 was related to the formation of Sn(IV) phases, which is not observed in relaxed defect configuration of interfacial ADs (Fig. 2) [41].

The charge neutral ID are created by shifting a Pb/Sn atom from their original position to an interstitial site. The charged ID are created by introducing an additional Pb/Sn atom at the interstitial position. We find that the charge neutral ID relaxes back to the pristine interface and are as such not stable. Charged ID exhibit similar behavior as that of Pb/Sn AD defects where the additionally introduced Pb (Sn) atom forms an interfacial structure with three bromine and one Pb (Sn) atom, respectively. The Pb-Br/Sn-Br bond length after relaxing the defect structure was found to be 2.95 Å and 2.89 Å for Pb and Sn ID, respectively.

In case of charged Pb/Sn ID (Fig. 3a & b), the additional dimer bond formed between Pb/Sn atoms lead to the formation of a mid-bandgap state. The IPR value for charged Pb/Sn ID is found to be 29/25 (compared to 4 for pristine interface) which is indicative of the strong charge localization happening at the defective site. A similar dimer formation due to the presence of interstitial Pb defect was also reported in the case of $MAPbI_3$ due to its strong covalent nature [42]. The formation and strength of these covalent bonds is in competition with the structural distortion and defect chemical state, respectively [43]. Similar observations are reported in literature for $CsPbBr_3$ where the presence of excess lead atoms at the surface was found to form a Pb dimer resulting in the formation of a deep hole trap [44].

A charged interstitial halide defect also leads to a large degree of structural rearrangement at the interface (Fig. 3c). The interstitial halide relocates from its initial position to the plane of Pb-Br-Sn bond, pushing down the Br atom located in between the interfacial Pb and Sn and forms a double bridge configuration at the interface. The formation of double bridge configuration by interstitial halide atoms coordinated by Pb atoms has been previously reported in $MAPbI_3/Br_3$ and was found to be unstable when the fermi energy was close to the valence band maximum [45]. It was reported that interstitial bromine ion can recreate a tin environment of Sn (IV) phases, but the DOS shows that halide ID does not create any detrimental state in the bandgap (Fig. 3c) [41].

Compared to interfacial halide ID, the creation of halide VD results in a minimal interfacial rearrangement of atoms. The Br mediated bond length between interfacial neighboring cations Pb-Sn was 5.98 Å at the pristine interface. After creation of VD, the distance between the neighboring B site cations reduce to 3.73 Å. The reduction in interatomic distance results in an enhanced covalent interaction between interfacial Pb-Sn atoms leading to the formation of a mid-bandgap state with defect localization properties (Fig. 4a). This is further corroborated by the wavefunction visualization shown in Fig. 4a (top right inset image). The calculated IPR value is 29 for the VD at the $MAPbBr_3$-$MASnBr_3$ interface compared to 4 for the pristine interface, suggesting that the wavefunction is highly localized for halide VD. Preceding studies have shown that the creation of a halide VD results in covalent interaction between the neighboring B site cations leading to the formation of a deep donor level (DX centre) [39]. In contrast to a halide ID, the presence of interfacial Pb/Sn VD does not result in the formation of any mid bandgap state as observed in Fig. 4b.

Previous reports suggest that the bromine substitution in $MAPbI_3$ results in higher formation energies for vacancy defects and reduces the migration of methylammonium ions due to lattice contraction; thus resulting in better efficiencies and stabilities [9,46]. In case of Br based perovskites, Pb interstitials forming Pb dimers was found to be the dominant source of defects and consequently a Br rich growth environment was suggested for them [47]. The necessity of circumventing the Pb content associated toxicity led to the development of Sn and mixed Pb/Sn based perovskite solar cells where they were found to exhibit perfectly balanced charge carrier transport [38]. Mixed perovskites were found to exhibit an intermediate behavior regarding their defect chemistry compared to their Pb/Sn counterparts and were

predicted to be potentially free of deep traps [48]. The introduction of Sn into PSC architecture introduces an additional bottleneck of ambient atmosphere Sn oxidation. Theoretical studies showed that the oxidation process was energetically unfavorable in the bulk Sn perovskite and was highly favorable at the surface. Hence surface passivation was proposed as an effective strategy to obtain stable and efficient Sn based PSCs [41]. Recently, a multitude of all bulk phase (3D) perovskite-perovskite interface are experimentally fabricated and their ambient atmosphere stability is studied. Among studied interfaces, $MAPbBr_3$-$MASnBr_3$ interface are found to be stable for more than 1500 h [19]. From our study it is observed that the all 3D Pb-Sn perovskite interface is highly prone to defect formation and localization of charge carriers. Adopting a halide rich synthesis condition can reduce the probability of formation of charge trapping halide vacancy and Pb/Sn interstitial defects thereby opening a pathway to further enhance the inherent stability demonstrated by the interface.

4. Conclusions

In conclusion, we have investigated the effect of interfacial defects on the electronic properties of an all 3D Pb-Sn perovskite interface. We found that Pb/Sn antisite defects do not result in the formation of midgap states. The relaxed defect configurations suggest that these defects are not stable and relaxes to form a Pb/Sn ID and a halide VD. Charged ID leads to a large interfacial structural rearrangement resulting in the formation of mid bandgap states by the creation of Pb/Sn dimer bonds. Formation of halide VD results in an enhanced covalent interaction between the interfacial neighboring B site cations leading to a charge localizing mid band gap state.

Our results show that, even though interfacing $MASnBr_3$ with $MAPbBr_3$ can significantly reduce the Sn oxidation, the associated interfacial defects can significantly affect the charge transfer across the interface. The presence of excess Pb/Sn or absence of halide ion at the interface can lead to detrimental charge trapping states which points to the fact that a Br excess synthesis environment is highly essential to further enhance the stability and performance of $MAPbBr_3$/$MASnBr_3$ interface.

CRediT authorship contribution statement

Sundheep R: Conceptualization, Data curation, Writing – original draft, Writing – review & editing. **Ankit Jain:** Conceptualization, Methodology, Supervision, Writing – review & editing.

Declaration of Competing Interest

The authors declare that they have no known competing financial interests or personal relationships that could have appeared to influence the work reported in this paper.

References

[1] S. Chen, X. Xiao, H. Gu, J. Huang, Iodine reduction for reproducible and high-performance perovskite solar cells and modules, Sci. Adv. 7 (2021) 1–7, https://doi.org/10.1126/sciadv.abe8130.

[2] J.J. Yoo, G. Seo, M.R. Chua, T.G. Park, Y. Lu, F. Rotermund, Y.K. Kim, C.S. Moon, N.J. Jeon, J.P. Correa-Baena, V. Bulović, S.S. Shin, M.G. Bawendi, J. Seo, Efficient perovskite solar cells via improved carrier management, Nature 590 (2021) 587–593, https://doi.org/10.1038/s41586-021-03285-w.

[3] Y.H. Kim, S. Kim, A. Kakekhani, J. Park, J. Park, Y.H. Lee, H. Xu, S. Nagane, R. B. Wexler, D.H. Kim, S.H. Jo, L. Martínez-Sarti, P. Tan, A. Sadhanala, G.S. Park, Y. W. Kim, B. Hu, H.J. Bolink, S. Yoo, R.H. Friend, A.M. Rappe, T.W. Lee, Comprehensive defect suppression in perovskite nanocrystals for high-efficiency light-emitting diodes, Nat. Photonics 15 (2021) 148–155, https://doi.org/10.1038/s41566-020-00732-4.

[4] W. Sun, Y. Liu, G. Qu, Y. Fan, W. Dai, Y. Wang, Q. Song, J. Han, S. Xiao, Lead halide perovskite vortex microlasers, Nat. Commun. 11 (2020), https://doi.org/10.1038/s41467-020-18669-1.

[5] Y. Xu, X. Wang, Y. Pan, Y. Li, E. Emeka Elemike, Q. Li, X. Zhang, J. Chen, Z. Zhao, W. Lei, Perovskite photodetectors based on p-i-n junction with epitaxial electron-blocking layers, Front. Chem. 8 (2020) 1–8, https://doi.org/10.3389/fchem.2020.00811.

[6] C. Li, H. Wang, F. Wang, T. Li, M. Xu, H. Wang, Z. Wang, X. Zhan, W. Hu, L. Shen, Ultrafast and broadband photodetectors based on a perovskite/organic bulk heterojunction for large-dynamic-range imaging, Light Sci. Appl. 9 (2020), https://doi.org/10.1038/s41377-020-0264-5.

[7] S.P. Senanayak, M. Abdi-Jalebi, V.S. Kamboj, R. Carey, R. Shivanna, T. Tian, G. Schweicher, J. Wang, N. Giesbrecht, D. Di Nuzzo, H.E. Beere, P. Docampo, D. A. Ritchie, D. Fairen-Jimenez, R.H. Friend, H. Sirringhaus, A general approach for hysteresis-free, operationally stable metal halide perovskite field-effect transistors, Sci. Adv. 6 (2020) 1–13, https://doi.org/10.1126/sciadv.aaz4948.

[8] H.F. Zarick, N. Soetan, W.R. Erwin, R. Bardhan, Mixed halide hybrid perovskites: a paradigm shift in photovoltaics, J. Mater. Chem. A 6 (2018) 5507–5537, https://doi.org/10.1039/c7ta09122b.

[9] L. McGovern, M.H. Futscher, L.A. Muscarella, B. Ehrler, Understanding the stability of MAPbBr3versus MAPbI3: suppression of methylammonium migration and reduction of halide migration, J. Phys. Chem. Lett. 11 (2020) 7127–7132, https://doi.org/10.1021/acs.jpclett.0c01822.

[10] E. Edri, S. Kirmayer, D. Cahen, G. Hodes, High open-circuit voltage solar cells based on organic-inorganic lead bromide perovskite, J. Phys. Chem. Lett. 4 (2013) 897–902, https://doi.org/10.1021/jz400348q.

[11] A. Mannodi-Kanakkithodi, J.S. Park, N. Jeon, D.H. Cao, D.J. Gosztola, A.B. F. Martinson, M.K.Y. Chan, Comprehensive computational study of partial lead substitution in methylammonium lead bromide, Chem. Mater. (2019), https://doi.org/10.1021/acs.chemmater.8b04017.

[12] M.T. Hörantner, T. Leijtens, M.E. Ziffer, G.E. Eperon, M.G. Christoforo, M. D. McGehee, H.J. Snaith, The potential of multijunction perovskite solar cells, ACS Energy Lett. 2 (2017) 2506–2513, https://doi.org/10.1021/acsenergylett.7b00647.

[13] S. Ippili, V. Jella, J. Kim, S. Hong, S.G. Yoon, Unveiling predominant air-stable organotin bromide perovskite toward mechanical energy harvesting, ACS Appl. Mater. Interfaces 12 (2020) 16469–16480, https://doi.org/10.1021/acsami.0c01331.

[14] C. Li, Z. Song, D. Zhao, C. Xiao, B. Subedi, N. Shrestha, M.M. Junda, C. Wang, C. S. Jiang, M. Al-Jassim, R.J. Ellingson, N.J. Podraza, K. Zhu, Y. Yan, Reducing saturation-current density to realize high-efficiency low-bandgap mixed tin–lead halide perovskite solar cells, Adv. Energy Mater. 9 (2019) 1–9, https://doi.org/10.1002/aenm.201803135.

[15] W.G. Choi, C.G. Park, Y. Kim, T. Moon, Sn perovskite solar cells via 2D/3D bilayer formation through a sequential vapor process, ACS Energy Lett. 5 (2020) 3461–3467, https://doi.org/10.1021/acsenergylett.0c01887.

[16] S. Shao, J. Liu, G. Portale, H.H. Fang, G.R. Blake, G.H. ten Brink, L.J.A. Koster, M. A. Loi, Highly reproducible Sn-based hybrid perovskite solar cells with 9% efficiency, Adv. Energy Mater. 8 (2018), https://doi.org/10.1002/aenm.201702019.

[17] Y. Lv, Y. Shi, X. Song, J. Liu, M. Wang, S. Wang, Y. Feng, S. Jin, C. Hao, Bromine doping as an efficient strategy to reduce the interfacial defects in hybrid two-dimensional/three-dimensional stacking perovskite solar cells, ACS Appl. Mater. Interfaces 10 (2018) 31755–31764, https://doi.org/10.1021/acsami.8b09461.

[18] C. Li, Z. Song, C. Chen, C. Xiao, B. Subedi, S.P. Harvey, N. Shrestha, K.K. Subedi, L. Chen, D. Liu, Y. Li, Y.W. Kim, C. sheng Jiang, M.J. Heben, D. Zhao, R. J. Ellingson, N.J. Podraza, M. Al-Jassim, Y. Yan, Low-bandgap mixed tin–lead iodide perovskites with reduced methylammonium for simultaneous enhancement of solar cell efficiency and stability, Nat. Energy 5 (2020) 768–776, https://doi.org/10.1038/s41560-020-00692-7.

[19] C.P. Clark, J.E. Mann, J.S. Bangsund, W.J. Hsu, E.S. Aydil, R.J. Holmes, Formation of stable metal halide perovskite/perovskite heterojunctions, ACS Energy Lett. 5 (2020) 3443–3451, https://doi.org/10.1021/acsenergylett.0c01609.

[20] M. Lai, A. Obliger, D. Lu, C.S. Kley, C.G. Bischak, Q. Kong, T. Lei, L. Dou, N. S. Ginsberg, D.T. Limmer, P. Yang, Intrinsic anion diffusivity in lead halide perovskites is facilitated by a soft lattice, Proc. Natl. Acad. Sci. U. S. A. 115 (2018) 11929–11934, https://doi.org/10.1073/pnas.1812718115.

[21] E. Shi, B. Yuan, S.B. Shiring, Y. Gao, Y.Guo Akriti, C. Su, M. Lai, P. Yang, J. Kong, B. M. Savoie, Y. Yu, L. Dou, Two-dimensional halide perovskite lateral epitaxial heterostructures, Nature 580 (2020) 614–620, https://doi.org/10.1038/s41586-020-2219-7.

[22] D.H. Kang, S.G. Kim, Y.C. Kim, I.T. Han, H.J. Jang, J.Y. Lee, N.G. Park, CsPbBr3/CH3NH3PbCl3Double layer enhances efficiency and lifetime of perovskite light-emitting diodes, ACS Energy Lett. 5 (2020) 2191–2199, https://doi.org/10.1021/acsenergylett.0c01036.

[23] S. Gu, R. Lin, Q. Han, Y. Gao, H. Tan, J. Zhu, Tin and mixed lead–tin halide perovskite solar cells: progress and their application in tandem solar cells, Adv. Mater. 32 (2020) 1–16, https://doi.org/10.1002/adma.201907392.

[24] J. Chang, G. Wang, Y. Huang, X. Luo, H. Chen, New insights into the electronic structures and optical properties in the orthorhombic perovskite MAPbI3: a mixture of Pb and Ge/Sn, New J. Chem. 41 (2017) 11413–11421, https://doi.org/10.1039/C7NJ01442B.

[25] J. Chang, H. Chen, G. Wang, B. Wang, X. Chen, H. Yuan, Electronic and optical properties of perovskite compounds MA1-: αFAαPbI3- βXβ (X = Cl, Br) explored for photovoltaic applications, RSC Adv. 9 (2019) 7015–7024, https://doi.org/10.1039/c8ra08189a.

[26] Y.S. Kim, C.H. Ri, U.H. Ko, Y.H. Kye, U.G. Jong, C.J. Yu, Interfacial enhancement of photovoltaic performance in MAPbI 3 /CsPbI 3 superlattice, ACS Appl. Mater. Interfaces (2021), https://doi.org/10.1021/acsami.0c22550.

[27] C. Liu, M. Hu, X. Zhou, J. Wu, L. Zhang, W. Kong, X. Li, X. Zhao, S. Dai, B. Xu, C. Cheng, Efficiency and stability enhancement of perovskite solar cells by

introducing CsPbI3 quantum dots as an interface engineering layer, NPG Asia Mater. 10 (2018) 552–561, https://doi.org/10.1038/s41427-018-0055-0.
[28] G. Kresse, J. Furthmu, Efficient iterative schemes for ab initio total-energy calculations using a plane-wave basis set¨, Phys. Rev. B 54 (1996) 11169–11186.
[29] P.E. Blochl, Projector augmented-wave method, Phys. Rev. B. 50 (1994) 17953–17979.
[30] S. Grimme, Semiempirical GGA-type density functional constructed with a long-range dispersion correction, J. Comput. Chem. 27 (2006) 1787–1799, https://doi.org/10.1002/jcc.
[31] M. Coduri, T.A. Strobel, M. Szafrański, A. Katrusiak, A. Mahata, F. Cova, S. Bonomi, E. Mosconi, F. De Angelis, L. Malavasi, Band gap engineering in MASnBr3 and CsSnBr3 perovskites: mechanistic insights through the application of pressure, J. Phys. Chem. Lett. 10 (2019) 7398–7405, https://doi.org/10.1021/acs.jpclett.9b03046.
[32] Q. Wen-Hu, C. Xue-Feng, Z. Jin, H. Jing-Hui, L. Hua, X. Qing-Feng, L. Na-Jun, C. Dong-Yun, Y. Zhi-Gang, L. Jian-Mei, Lead-free perovskite MASnBr3-based memristor for quaternary information storage, InfoMat 2 (2020) 743–751.
[33] C. Pashartis, O. Rubel, Localization of electronic states in III-V semiconductor alloys: a comparative study, Phys. Rev. Appl. 7 (2017) 1–12, https://doi.org/10.1103/PhysRevApplied.7.064011.
[34] C. Zheng, O. Rubel, M. Kepenekian, X. Rocquefelte, C. Katan, Electronic properties of Pb-I deficient lead halide perovskites, J. Chem. Phys. 151 (2019), https://doi.org/10.1063/1.5127513.
[35] D. Niesner, Surface electronic structure and dynamics of lead halide perovskites, APL Mater. 8 (2020), https://doi.org/10.1063/5.0019877.
[36] J.I.J. Choi, M.E. Khan, Z. Hawash, H. Lee, L.K. Ono, Y. Qi, Y.H. Kim, J.Y. Park, Surface termination-dependent nanotribological properties of single-crystal MAPbBr3 surfaces, J. Phys. Chem. C 124 (2020) 1484–1491, https://doi.org/10.1021/acs.jpcc.9b10191.
[37] R. Sundheep, A. Jain, Contact passivation for defect mitigation in multi-dimensional perovskite interfaces, Appl. Phys. Lett. 119 (2021), https://doi.org/10.1063/5.0061908.
[38] E. Mosconi, P. Umari, F. De Angelis, Electronic and optical properties of mixed Sn-Pb organohalide perovskites: a first principles investigation, J. Mater. Chem. A 3 (2015) 9208–9215, https://doi.org/10.1039/c4ta06230b.
[39] Y. Liang, X. Cui, F. Li, C. Stampfl, S.P. Ringer, R. Zheng, First-principles investigation of intrinsic point defects in perovskite CsSnBr 3, Phys. Rev. Mater. 5 (2021) 1–10, https://doi.org/10.1103/physrevmaterials.5.035405.
[40] J. Kim, C.H. Chung, K.H. Hong, Understanding of the formation of shallow level defects from the intrinsic defects of lead tri-halide perovskites, Phys. Chem. Chem. Phys. 18 (2016) 27143–27147, https://doi.org/10.1039/c6cp02886a.
[41] D. Ricciarelli, D. Meggiolaro, F. Ambrosio, F. De Angelis, Instability of tin iodide perovskites: bulk p-doping versus surface tin oxidation, ACS Energy Lett. 5 (2020) 2787–2795, https://doi.org/10.1021/acsenergylett.0c01174.
[42] M.L. Agiorgousis, Y.Y. Sun, H. Zeng, S. Zhang, Strong covalency-induced recombination centers in perovskite solar cell material CH3NH3PbI3, J. Am. Chem. Soc. 136 (2014) 14570–14575, https://doi.org/10.1021/ja5079305.
[43] Z. Zhang, L. Qiao, C. Mora-Perez, R. Long, O.V. Prezhdo, Pb dimerization greatly accelerates charge losses in MAPbI3: time-domain ab initio analysis, J. Chem. Phys. 152 (2020), https://doi.org/10.1063/1.5131342.
[44] L. Qiao, R. Long, W.H. Fang, Surface Pb-dimer passivated by molecule oxygen notably suppresses charge recombination in CsPbBr3 perovskites: time-domain ab initio analysis, J. Phys. Chem. Lett. 10 (2019) 5499–5506, https://doi.org/10.1021/acs.jpclett.9b02201.
[45] S.G. Motti, D. Meggiolaro, S. Martani, R. Sorrentino, A.J. Barker, F. De Angelis, A. Petrozza, Defect activity in lead halide perovskites, Adv. Mater. 31 (2019) 1–11, https://doi.org/10.1002/adma.201901183.
[46] J.H. Noh, S.H. Im, J.H. Heo, T.N. Mandal, S. Il Seok, Chemical management for colorful, efficient, and stable inorganic-organic hybrid nanostructured solar cells, Nano Lett. 13 (2013) 1764–1769, https://doi.org/10.1021/nl400349b.
[47] A. Buin, R. Comin, J. Xu, A.H. Ip, E.H. Sargent, Halide-dependent electronic structure of organolead perovskite materials, Chem. Mater. 27 (2015) 4405–4412, https://doi.org/10.1021/acs.chemmater.5b01909.
[48] D. Meggiolaro, D. Ricciarelli, A.A. Alasmari, F.A.S. Alasmary, F. De Angelis, Tin versus lead redox chemistry modulates charge trapping and self-doping in tin/lead iodide perovskites, J. Phys. Chem. Lett. 11 (2020) 3546–3556, https://doi.org/10.1021/acs.jpclett.0c00725.